Geophysical Journal International

Geophys. J. Int. (2018) **214,** 474–484
Advance Access publication 2018 April 19
GJI Seismology

doi: 10.1093/gji/ggy155

ISC-EHB: reconstruction of a robust earthquake data set

J. Weston,[1] E.R. Engdahl,[2] J. Harris,[1] D. Di Giacomo[1] and D.A. Storchak[1]

[1] *International Seismological Centre, Thatcham, Berkshire RG19 4NS, UK. E-mail: isc-ehb@isc.ac.uk*
[2] *Department of Physics, University of Colorado, Boulder, CO 80309-0390, USA*

Accepted 2018 April 18. Received 2018 April 14; in original form 2018 February 12

SUMMARY

The Engdahl-van der Hilst-Buland (EHB) Bulletin of hypocentres and associated traveltime residuals was originally developed with procedures described by (Engdahl *et al*. 1998) and ended in 2008. It is a widely used seismological data set, which is now expanded and reconstructed, partly by exploiting updated procedures at the International Seismological Centre (ISC), to produce the ISC-EHB. The reconstruction begins in the modern period (2000–2013) to which new and more rigorous procedures for event selection, data preparation, processing and relocation are applied. The selection criteria minimize the location bias produced by unmodelled 3-D Earth structure, resulting in events that are relatively well-located in any given region. Depths of the selected events are significantly improved by a more comprehensive review of near station and secondary phase traveltime residuals based on ISC data, especially for the depth phases pP, pwP and sP, as well as by a rigorous review of the event depths in subduction zone cross-sections. The resulting cross-sections and associated maps are shown to provide details of seismicity in subduction zones in much greater detail than previously achievable. The new ISC-EHB data set will be especially useful for global seismicity studies and high-frequency regional and global tomographic inversions.

Key words: Seismology; Seismicity and tectonics; Subduction zone processes.

1 INTRODUCTION

Earthquake bulletins are valuable tools for investigating and understanding seismicity and tectonic structures across local, regional and global scales. The Engdahl–Van der Hilst–Buland Bulletin (hereafter referred to as the EHB) is one such bulletin that consists of more than 140 000 earthquake hypocentres and associated phase arrival times for teleseismically well-constrained events that have been selected from the International Seismological Centre (ISC 2018) Bulletin, and relocated with a focus on the depth resolution of the events. This high depth resolution is the main factor behind the EHB being widely used by the seismological community for a wide range of research topics: global and regional tomography (e.g. Montelli *et al.* 2004; Huang & Zhao 2006; Li *et al.* 2008; Schmid *et al.* 2008) and regional tectonic studies (e.g. Hayes *et al.* 2012; Pesicek *et al.* 2012; Waldhauser *et al.* 2012; Duarte & Schellart 2016).

Following the expansion of both global and regional seismic networks the volume of data available to the ISC has significantly increased, as has the quality of data with improvements in the capabilities of instrumentation. This is the motivation behind an update of the EHB methodology, in conjunction with the ISC, to develop the ISC-EHB. With improved data and procedures, we now aim to refine and update this database for future applications. It should be noted that while the focus of this paper is the ISC-EHB, two other ISC products are mentioned: the ISC Bulletin and ISC-GEM catalogue. All three products suit different research needs and to provide clarity for the reader we outline them here. The ISC Bulletin is the main product of the ISC, it is a comprehensive global summary of natural and anthropogenic events, which can be used for a wide range of purposes as it contains all of the data reported to the (ISC). ISC-GEM is an extensive list of moderate to large global earthquakes selected from the ISC Bulletin, where the focus is on homogeneous estimates for location and magnitude, which makes it useful for seismic hazard and risk modelling, as well as earthquake forecasting (Storchak *et al*. 2015). The ISC-GEM catalogue closely replicates the ISC-EHB for events of M 5.5 and larger but the two catalogues should be used independently as they are meant for different applications. For further details on all ISC products we refer the reader to www.isc.ac.uk/products.

This paper outlines the revised event selection, data preparation and processing, and relocation procedures that have been tested and conducted to produce the ISC-EHB. This includes an improved and more rigorous analysis of reported depth phases, utilizing both automatic and manual review for robust depth determination. The new procedure has been applied to events between 2000 and 2013 and this data set is available in RES and HDF formats, as well as being available to interactively search (www.isc.ac.uk/isc-ehb).

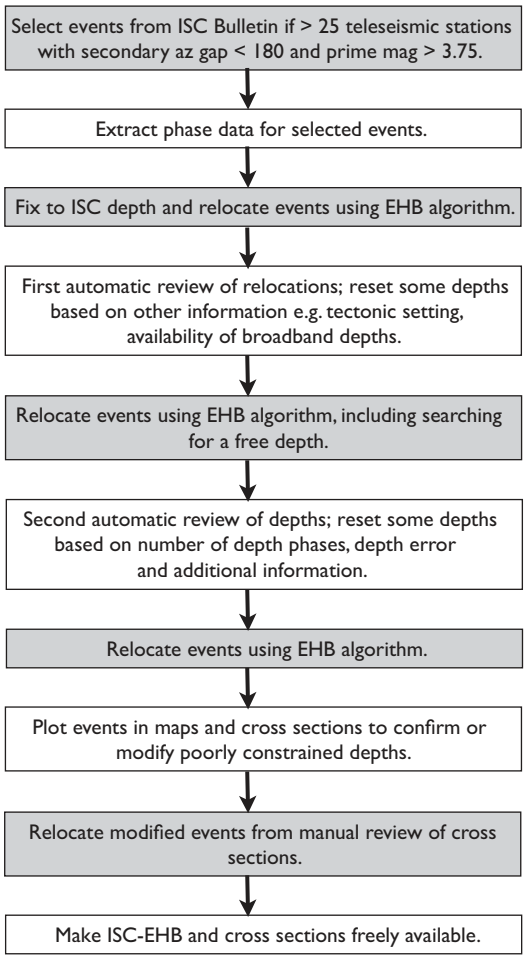

Figure 1. Flowchart depicting the semi-automatic process for selection, relocation and review of events for the ISC-EHB data set.

2 DATA AND METHODS

The new ISC-EHB procedures are guided by those used for the EHB bulletin, with the aim of developing an increasingly automated and more robust process. Fig. 1 provides an overview of all the steps behind the construction of the ISC-EHB, which are described in more detail in the following subsections.

2.1 Selection and preparation

The first step in creating the ISC-EHB is the selection of teleseismically well-constrained events from the ISC Bulletin (ISC, 2018). This criterion for selection is important for reducing the bias in hypocentre determination regionally. Due to the improvement in quality and number of seismic stations, there are now many more teleseismically well-constrained events and associated phases to review. For example, for the ISC-GEM (Storchak *et al.* 2015), which is similar to the ISC-EHB in that it involves the selection and relocation of events from the ISC Bulletin, the median number of phases and stations per event has consistently increased since the 1960s (Fig. 2). Following the year 2000, the rate of increase rises significantly. Therefore, we have implemented a stricter event selection criterion that is based on what was used for the original EHB (Engdahl *et al.* 1998).

Originally the number of teleseismic stations, secondary teleseismic azimuthal gap (largest azimuthal gap filled by a single station; Bondar *et al.* 2004) and magnitude were used to select events. We tested various combinations of the three aforementioned factors, whereby the minimum number of teleseismic stations was allowed to vary between 15 and 30, the maximum allowed secondary teleseismic azimuthal gap varied between 160° and 180° and the minimum prime magnitude (Di Giacomo & Storchak 2016) varied between 3.0 and 4.5. The prime magnitude is simply the best-suited magnitude for an event among widespread magnitude types (M_w, M_s, m_b or local types such as M_{JMA}, M_L, m_{bLg}, M_D, in this order). Following these tests, we reached a criterion that balanced the number of well-constrained events and the number of small magnitude ($M < 4.5$) events. Thus, events are selected from the ISC Bulletin if they meet the following two criteria:

(1) The event has >25 teleseismic (>28°) stations with a secondary teleseismic azimuthal gap < 180° .
(2) The prime magnitude is >3.75, where the prime magnitude is the magnitude selected by the ISC following Di Giacomo & Storchak (2016).

This approach for selection criteria is one way of reducing regional bias in hypocentre determination due to unmodelled 3-D Earth structure and the distribution of seismic stations (Engdahl *et al.* 1998; Bondar *et al.* 2004). This selection criterion was applied to events between 2000 and 2013 in the ISC Bulletin. This time period was chosen, first because it is around the year 2000 that there is a sharp increase in the data available (Fig. 2). Second, we extended beyond 2008 (when the original EHB stopped) and up to 2013 because we select events from the reviewed ISC Bulletin, which at the time of selecting events the most recent and complete reviewed year was 2013. Once the events are selected, the event hypocentral parameters and the associated phases were compiled into the input FFB (Fixed Format Bulletin) file required for EHB relocation.

2.2 Relocation

The EHB algorithm described in Engdahl *et al.* (1998) is used to relocate the events. This algorithm uses traveltime tables derived from a recently developed 1-D Earth model and uses *P*, *S* and other later arriving phases in the location procedure. We use the Earth model ak135 (Kennett *et al.* 1995), now utilized by international agencies, such as the ISC and NEIC, for the routine location of earthquakes globally. The location procedure uses the arrival times for first-arriving *P* and *S* phases, core phases (PcP and PKP) and depth phases (pP, a reflection off the ocean surface pwP and sP). These phases are corrected for lateral variations in upper-mantle velocities (patch corrections, see Engdahl *et al.* 1968) and elevation beneath stations, for topography/water at depth phase bounce points and for the Earth's ellipticity. By far the most significant improvements provided by the EHB location procedure are in-depth determination by interpreting and utilizing the teleseismic depth phases pP, pwP and sP. These depth phases and PcP, that are re-identified at each iteration using a statistical procedure described in Engdahl *et al.* (1998), provide powerful constraints on focal depth.

The EHB algorithm is run numerous times throughout the ISC-EHB process, at least three times during the automatic review, and a final time after the manual review of events. It is likely to be run more than four times though, for reasons that are discussed in the following subsections.

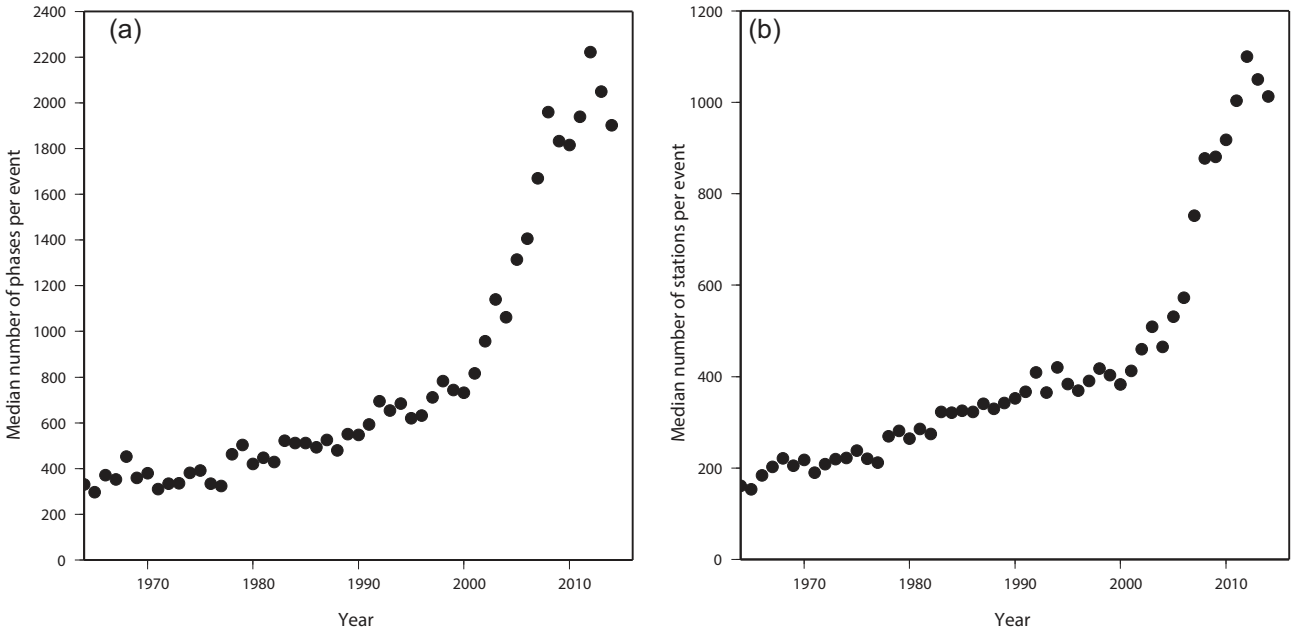

Figure 2. (a) Number of phases per ISC-GEM event (ISC-GEM, www.isc.ac.uk/iscgem, Storchak *et al.* 2015 and references therein), shown as a median yearly value. (b) Number of stations per ISC-GEM event, calculated as median yearly value. ISC-GEM is chosen as it contains mostly well-determined events $M_w > 5.5$ and the number of these events remains relatively consistent over the time period plotted here.

2.3 Automatic review

There are two rounds of automatic review, whereby each event depth is systemically reviewed. This involves running a script that determines if each event meets a certain criterion, which are different for the first and second automatic reviews. The main purpose of these automatic reviews is to reduce the number of events that may need assessing in the subsequent manual review.

Prior to the first automatic review, the ISC starting locations and depths (Bondar & Storchak 2011) are used to compute fixed depth EHB relocations. This first run of the EHB algorithm is carried out in order to re-determine the phase identifications and residuals. In the first automatic review the focus is on resetting depths based on two factors: the tectonic setting and information from other catalogues or previously published studies. For events that are in a ridge or open ocean setting the depth is reset to 10 km. All events within a 55 km spherical radius of trenches or volcanoes have the depth reset to 15 km, and depths for events within regions of known shallow seismicity are also reset to 15 km. Following this, a search is carried out for any events that appear in either the ISC-GEM catalogue (Storchak *et al.* 2015), have USGS broad-band depths (Choy & Engdahl 1987) or have been relocated in previously published studies (e.g. Engdahl *et al.* 2006). The depths are set to the values reported by these sources, and in instances where the event appears in more than one of these sources preference is given to the USGS broad-band value, followed by ISC-GEM and finally published studies. Moreover, the prior knowledge takes preference over the tectonic setting, so if, for example, we have a depth from a catalogue or study for a volcanic event, we will use the reported value rather than setting it to 15 km. These assumptions regarding tectonic setting and prior knowledge may not be universally accurate, but the minor number of errors as a result of this will most likely be corrected in the subsequent manual review.

The events are then relocated again using the EHB algorithm, and the depth and location are allowed to vary for all events. Next, in the second automatic review, we take into account the depth error and the number of depth phases used to constrain the hypocentral parameters, hereafter referred to as defining depth phases. This is in addition to considering the tectonic setting and prior knowledge. For any ridge or open ocean events that have less than three defining depth phases and a depth error > 5 km the depth is fixed to 10 km. The same applies to continental, trench or volcanic events except the depth is set to 15 km. Similarly, events with ISC-GEM, USGS broad-band depths or depths from special studies are fixed to the reported depths if they have less than three defining depth phases and a depth error larger than 5 km. Any remaining events that have a GCMT solution are set to the GCMT depth, these, and all other events that do not meet any of the prior criteria are allowed to vary in both depth and location in the subsequent relocation. The EHB algorithm is run again, and iterations continue until solutions for all events become stable, typically this takes two to three iterations.

2.4 Manual review

The final stage of the ISC-EHB procedure involves the manual review of events in cross-sections. Globally we take each tectonic region or subduction zone, create arc centric sectors, with respect to a centre of curvature of the arc, based on either a fit to the curvature of the trench (S. Kirby, personal communication, 2012), volcanoes (Siebert & Simkin 2002) or intermediate events within the slab, and split them up into cross-sections. Fig. 3(a) shows the Marianas subduction zone split up into 17 cross-sections, where the ISC-EHB events are plotted as shallow, intermediate and deep earthquakes (yellow, orange and red circles, respectively, Fig. 3a). In each cross-section the ISC-EHB events are plotted with respect to their radius and azimuth, from the arc centre of curvature, within the sector without overlap, and events from the ISC-GEM catalogue for the 1900–1999 period (white circles, Fig. 3b) and any trench points and volcanoes are also plotted for reference (Siebert & Simkin 2002). The ISC-EHB events are plotted and coloured according to the depth category. We assign a depth category to each event, as an

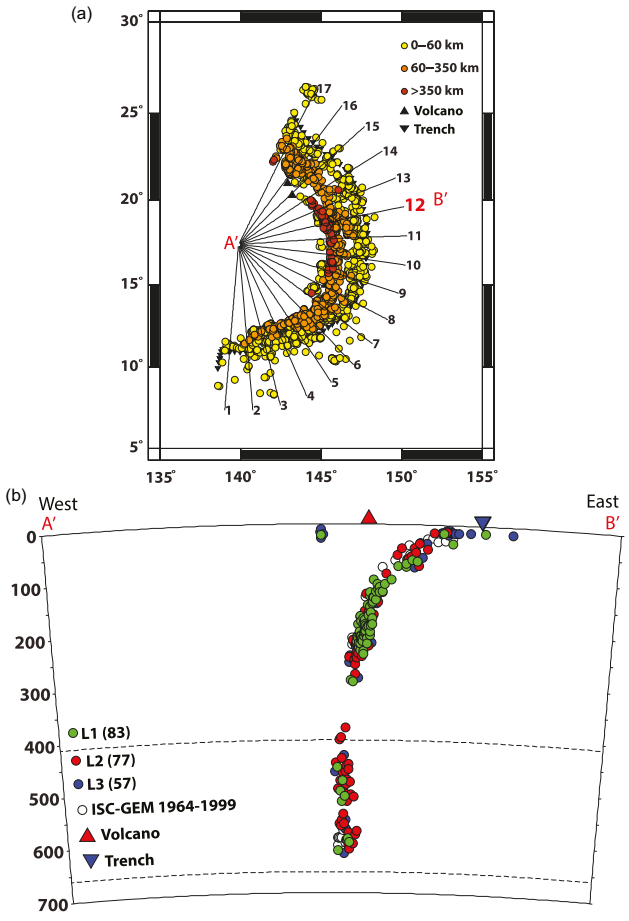

Figure 3. (a) Map of Marianas subduction zone split up into 17 cross-sections for manual review, with cross-section 12 highlighted in red. (b) Cross-section 12 denoted by A'-B' in (a). The green, red and blue circles are ISC-EHB events in L1, L2 and L3 depth categories, respectively. The number of each of these events is shown in brackets in the legend. White circles refer to events from the ISC-GEM catalogue. Red triangles denote volcanoes and inverted blue triangles show the location of the trench. The dashed lines refer to the 410 and 660 km discontinuities. Please note that all cross-sections in this study are plotted in true scale taking into account Earth curvature.

Table 1. Magnitude combinations in the ISC-EHB for 2000–2013.

Magnitude types	Number of events
m_b	29 852
m_b, M_s, M_w	17 034
m_b, M_s	16 993
m_b, M_w	5141
M_s, M_w	1
None	6

indication of the level of constraint on the depth. The categories are based on the depth error, number of phases and whether the depth is based on the phase data (free depth) or the depth is fixed. There are three categories as follows:

(1) Level 1 (L1)—An event with a free depth with a standard depth error < 5 km and at least three defining depth phases, or an event with a fixed depth that is well-constrained by depth phases or by a USGS broad-band depth; indicated by the green circles in Fig. 3(b).

ISC evid 601112121 | Event time: yr m d 6 10, h m s 13 32 55.57 | DEQ d iter = 2 | lat = 18.715 lon = 145.684 depth = 153.9 0.0 smdel = 0.000

Station	Delta deg.	Azimuth	Phase Identification: EHB	ISC	Agency	Phase arrival time	Phase Residuals: Selected	pP	pwP	sP	PcP
HIA	36.94	331.52	pwP	epP	epP	13 40 24.36	-1.82	2.5	-1.8	-14.6	
SONM	43.12	321.38	pP	pP	pP	13 41 14.58	0.51	0.5	-4.1		
ASAR	43.66	195.73	PcP	PcP	PP	13 42 29.20	0.88				0.9
LSA	50.53	293.37	pwP	epP	epP	13 42 18.44	0.39	5.8	0.4	-11.1	
MKAR	58.44	313.87	pP	pP	pP	13 43 8.40	-1.56	-1.6	-6.3		
KURK	61.25	318.10	pP	pP	pP	13 43 28.50	-0.66	-0.7	-5.5		-6.6
KURBB	61.30	317.99	pP	pP	pP	13 43 28.50	-0.99	-1.0	-5.8		-6.8
AAK	63.85	308.91	PcP	pP	pP	13 43 47.52	0.18	-0.8	-5.5		0.2
NIL	65.51	299.09	pwP	epP	e*PP	13 44 2.50	-0.87	4.1	-0.9	-12.3	9.1
BVAR	66.45	320.41	pP	pP	pP	13 44 3.04	-0.90	-0.9	-5.7		6.3
NVAR	83.14	51.88	pP	pP	pP	13 45 41.18	-1.71	-1.7	-6.1		
PDAR	87.82	45.45	pP	pP	pP	13 46 6.16	-0.06	-0.1	-4.2		
SUMG	88.89	1.25	pwP	epP	epP	13 46 13.76	0.04	3.0	0.0	-12.8	

Figure 4. Example of an event from the phase residual review file which is produced after relocation. The event shown is in cross-section 12 in the Marianas at 153 km depth in Fig. 3(b). Column headers are annotated in blue and red. The file only shows stations at less than 3° or greater than 28°. The phase identifications from ISC, EHB and the reporting agency are shown, as well as the residuals for the phases pP, sP, pwP and PcP.

(2) Level 2 (L2)—An event with a free depth with a standard depth error < 5 km and less than three defining depth phases or an event with a free depth and a standard depth error 5–15 km, or an event with a fixed depth based on the GCMT solution; indicated by the red circles in Fig. 3(b).

(3) Level 3 (L3)—An event with a free depth with a depth error > 15 km or an event with a fixed depth based on a review of local/nearby seismicity or tectonic constraints; indicated by the blue circles in Fig. 3(b).

Thus, L1 events are the most well-constrained depths and L3 are the least well-constrained. Currently, users are not able to search the database using the depth category criteria, but this will be implemented in the near future.

Events in each cross-section are manually reviewed to confirm their depths based on the relevant data or to modify the depths of any poorly constrained outliers based on the depths of nearby well-constrained events and/or the tectonic setting. For any events that do need reviewing we examine the phase residuals of near stations (primarily < 3°) and depth phases. An example snapshot of the file with these residuals for an event in the Marianas in Fig. 3(b) is shown in Fig. 4. The most common issues seen for events in this file, that lead to a depth being fixed or set at a new value, are overly positive or negative residuals, misidentified depth phases or few near stations and depths phases. If any of these are encountered and there are less than three defining depth phases then the depth is fixed to a value that agrees with surrounding events (usually in increments of 10 km). Alternatively, if there are more than three defining depth phases, then the depth is set to a value that agrees with surrounding events in order to try and obtain a free depth in the next run of the EHB algorithm. Following these modifications from this manual review the EHB algorithm is run again and the modified events are checked, and if necessary the algorithm is run again to arrive at stable solutions for all events. This produces the final version of the relocated data set, the ISC-EHB.

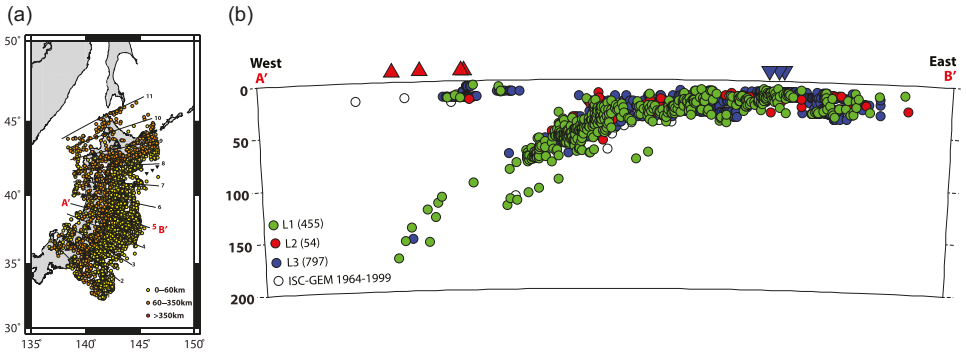

Figure 5. (a) Map of 11 cross-sections for the Honshu subduction zone, where number 5 (denoted by A'-B') is in the region of the hypocentre of the M_w 9.0 2011 March 11, Tohoku-oki earthquake. (b) Cross-section 5 including aftershocks of the M_w 9.0 event. Symbols and colours follow same convention as in Fig. 3.

2.5 Aftershock sequences

For large aftershock sequences there can be many events that meet the selection criteria, but they are not very well-constrained in depth. In this instance the depths of these events are set to that of nearest neighbours that have well-constrained depths, and are assigned the depth category L3. Fig. 5 is an example that includes many aftershocks of the M_w 9.0, 2011 March 11, Tohoku-oki earthquake, that were set to the depths of nearby well-constrained events. The observed double seismic zone is discussed in more detail in Section 4.5.

3 RESULTS

From the 69 655 events between 2000 and 2013, initially selected from the ISC Bulletin using the new criteria, 69 027 events remain after the new review procedure and make up the ISC-EHB. The global distribution of events (Fig. 6) shows that subduction zones dominate the data set and most plate tectonic margins are covered. It should be noted that there are 18 anthropogenic events in the data set, including induced events, mine explosions and rock bursts. These anthropogenic events are identified in the data set and can be removed if needed; further details are given in the FORMAT.HDF and FORMAT.RES files available from www.isc.ac.uk/isc-ehb.

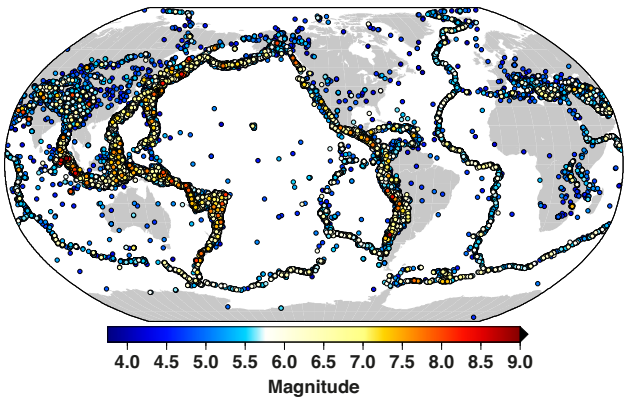

Figure 6. Global distribution of the 2000–2013 ISC-EHB events colour-coded by the largest magnitude value among M_w(GCMT), M_s/m_b(ISC). The magnitude content of the ISC-EHB bulletin is outlined in Section 3.1.

There are 30 720 events with free depth and the remaining 38 307 are fixed. In the data set there are 18 570 L1 events, 21 589 L2 events and 28 868 L3 events, the global distribution of events in each category is relatively similar (Fig. 7). The median formal depth error for L1 events is 1.65 km and for L2 events is 4.23 km. Notably there is a high number of L1 events on the mid-Atlantic ridge (Fig. 7a), which we think is due to the depth phases reported from North American and European stations. Conversely, there are fewer L1 events in the European and Mediterranean regions, probably because there are so few reported teleseismic depth phases available for these events.

3.1 Magnitude content

The EHB algorithm does not recompute any magnitudes, therefore the magnitudes given in the HDF and RES files are from other sources. Up to three magnitudes (with no author or uncertainty) can be listed: m_b, M_s and M_w, in this order. To keep the magnitude content clear and simple to use, we include only preferred m_b and M_s as determined by the ISC, and M_w from the GCMT. The most frequent magnitude is m_b (missing for six events only), followed by M_s (available for 34 028 events) and then M_w (22 176 events). The magnitude combinations are summarized in Table 1. Fig. 8 shows the cumulative counts for these three magnitude types in the ISC and ISC-EHB Bulletin. For the period 2000–2013 the global events ($M > \sim 5.5$) are usually well-recorded and are therefore included in the ISC-EHB Bulletin, as they meet the network selection criteria. Only 1544 events with M_w from GCMT (mostly below 5.3 and including surface wave locations only, see Ekström 2006) are not included in the ISC-EHB. It should be noted that for events between 2000 and 2009 the ISC magnitudes have been obtained prior to the introduction of the new ISC locator, and therefore will be updated in the future as part of the Rebuild project of the ISC Bulletin (Storchak *et al.* 2017).

3.2 Cross-sections

For the manual review we look at 89 different regions around the world, and there are 840 cross-sections in total, all of which are available for download from www.isc.ac.uk/isc-ehb/regions. The minimum number of cross-sections for a region is 1 and the maximum is 27 (Izu subduction zone). The majority of the regions are subduction zones and in many cases due to their length spanning hundreds sometimes thousands of kilometres, they have been divided into small subregions. For example, the subduction zone

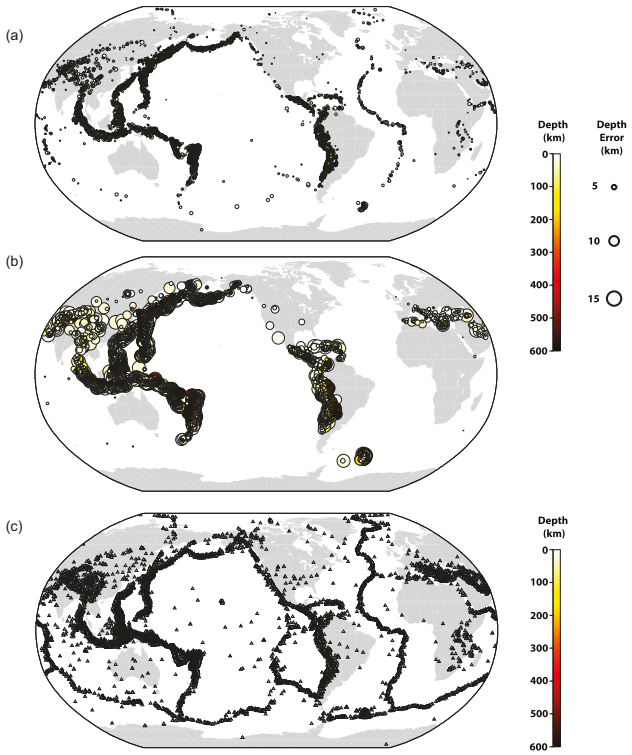

Figure 7. Global distribution of (a) 18 570 L1 ISC-EHB events and (b) 21 589 L2 ISC-EHB events, where circles are coloured according to event depth, and the size of the circle corresponds to the depth error. (c) Global distribution of 28 868 L3 ISC-EHB events, where the triangles are coloured according to depth and are all the same size as the majority of the events have fixed depths or the free depth has an error > 15 km.

along the South American coast is split up into seven smaller regions (Colombia South, Ecuador, Peru, Chile North, Chile Central and Chile South). One of these subregions at the Peru–Chile border is shown in Fig. 9.

3.3 Comparisons with other catalogues

Here, we compare L1 ISC-EHB depths with those reported in the GCMT catalogue, the ISC Bulletin and with USGS broad-band depths. In general there is good agreement between GCMT and ISC-EHB depths; the mean difference in depth is -0.8 ± 8.5 km (Fig. 10a). There is more scatter at shallower depths, which could be due to the fact that GCMT uses long-period data with poorer depth resolution. Moreover, the lineation at shallow depths is probably because for events with a GCMT default depth of 12 or 15 km the ISC-EHB depth is deeper. GCMT depths are also slightly larger than ISC-EHB depths for intermediate and deep events, which is probably due to the use of different velocity models with increasing depth. It should also be noted that GCMT depths are measuring the centroid rather than the hypocentre. There are fewer events in the USGS broad-band catalogue that uses the same global model (ak135) and the depths are based on the fit to measured differential times of depth phases. However, again there is good agreement between these depths and the ISC-EHB values; here the mean difference in depth is 4.2 ± 5.1 km (Fig. 10b). Comparing the ISC-EHB depths with those in the ISC Bulletin, there are many more events and the scatter is larger, and the mean difference in depth is -2.4 ± 7.3 km (Fig. 10c).

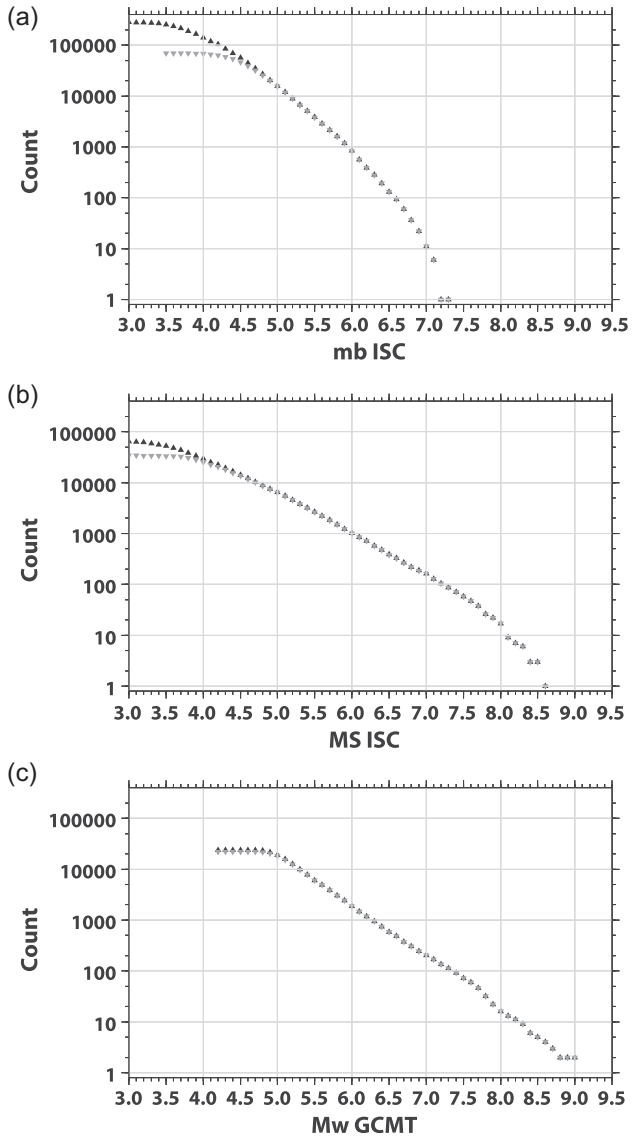

Figure 8. Cumulative number of events in bins of 0.1 magnitude units in the ISC Bulletin (black triangles) and in the ISC-EHB Bulletin (grey inverted triangles) for (a) the ISC preferred m_b, (b) the ISC preferred M_s and (c) the M_w from GCMT.

4 DISCUSSION

The main aim of the data set is to provide a resource for tomography as well as for global and regional tectonic studies. In this section we provide some comments on the limitations and observations of the data set.

4.1 1-D model limitations

Some bias in ISC-EHB hypocentres remains due to unmodelled lateral variations in velocities, mostly in subduction zones, which cannot be accounted for unless a 3-D Earth model is used for location. However, the selection criterion based on azimuthal gap minimizes this bias and at the very least distributes the effects uniformly where earthquakes are closely located (see also Bondar *et al.* 2004). The teleseismic bias in continental regions is examined by

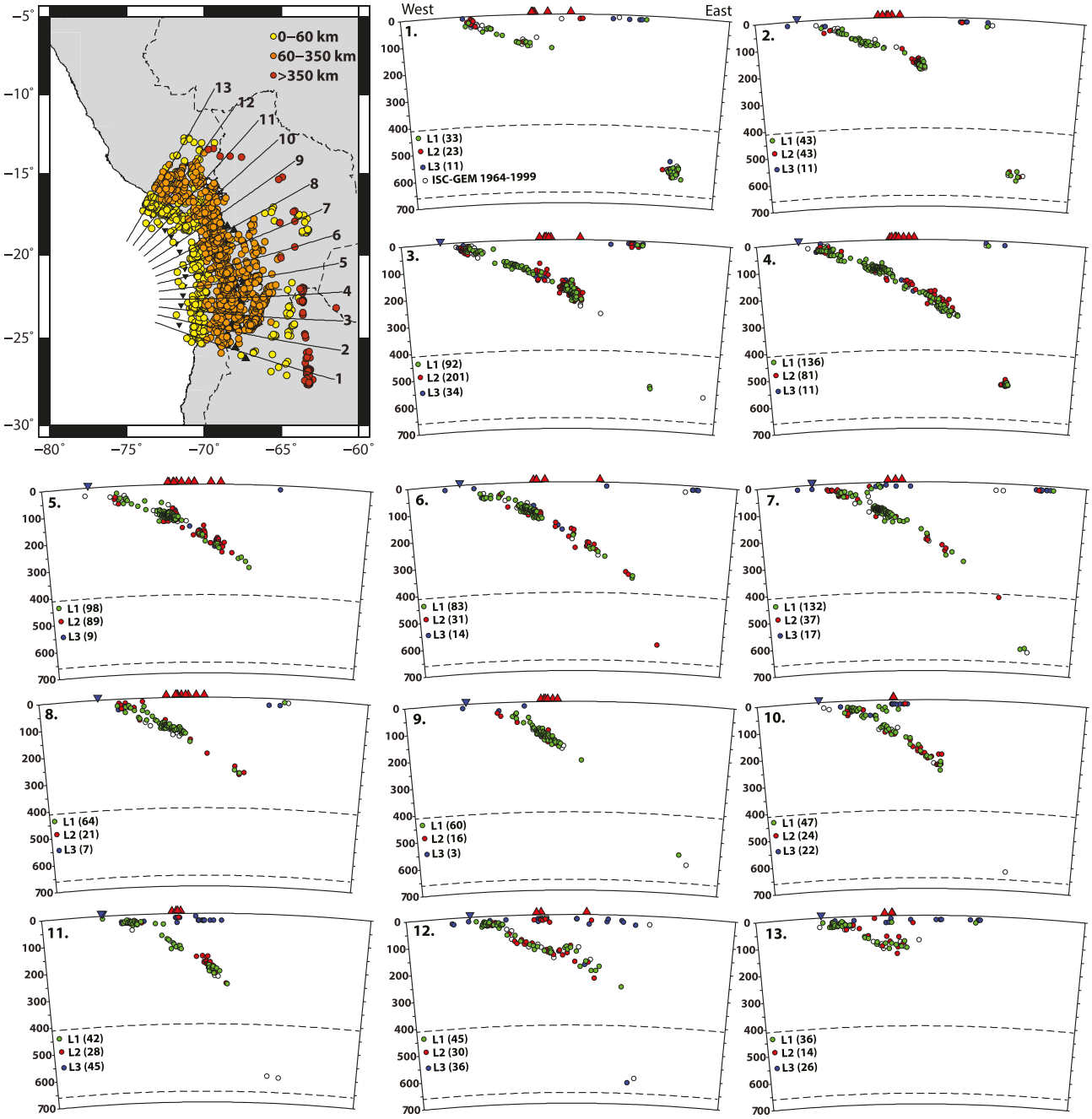

Figure 9. Map and 13 cross-sections for part of the subduction zone along the South America coast, near the Peru–Chile border. Symbols and colours follow the same convention as in Fig. 3. The west–east orientation of the cross-sections is highlighted in cross-section 1 to guide the reader.

comparing ISC-EHB locations with the same events reported in the IASPEI Ground Truth (GT) reference events list, which is almost entirely comprised of continental events and is compiled by the ISC (www.isc.ac.uk/gtevents). 150 events appear in both the ISC-EHB and GT reference events list, and the ISC-EHB locations are on average mislocated by 11.0 ± 5.4 km, somewhat less than the mislocation found by other authors using different selection criteria (Myers & Schultz 2000; Bondar *et al.* 2008). In any case, the bias is clearly much larger in subduction zones (Herrin & Taggart 1968) due to the traveltime bias introduced by high-velocity subducting slabs, even with good station coverage.

4.2 Depth uncertainties

ISC-EHB L1 depths are primarily constrained by depth phases, but close (<3°) stations, when available, are also quite useful in constraining depth when combined with the depth phases. Other later phases such as PcP and PKP are only useful in identifying gross errors in depth. In addition, one must realize that the standard error in depth used to categorize event depths is only a formal error that does not take into account the effects of lateral variations in velocity. Nevertheless, it does provide a useful measure of relative but not absolute depth uncertainty. Fig. 9 suggests that this relative depth uncertainty is probably no more than 15 km (two standard

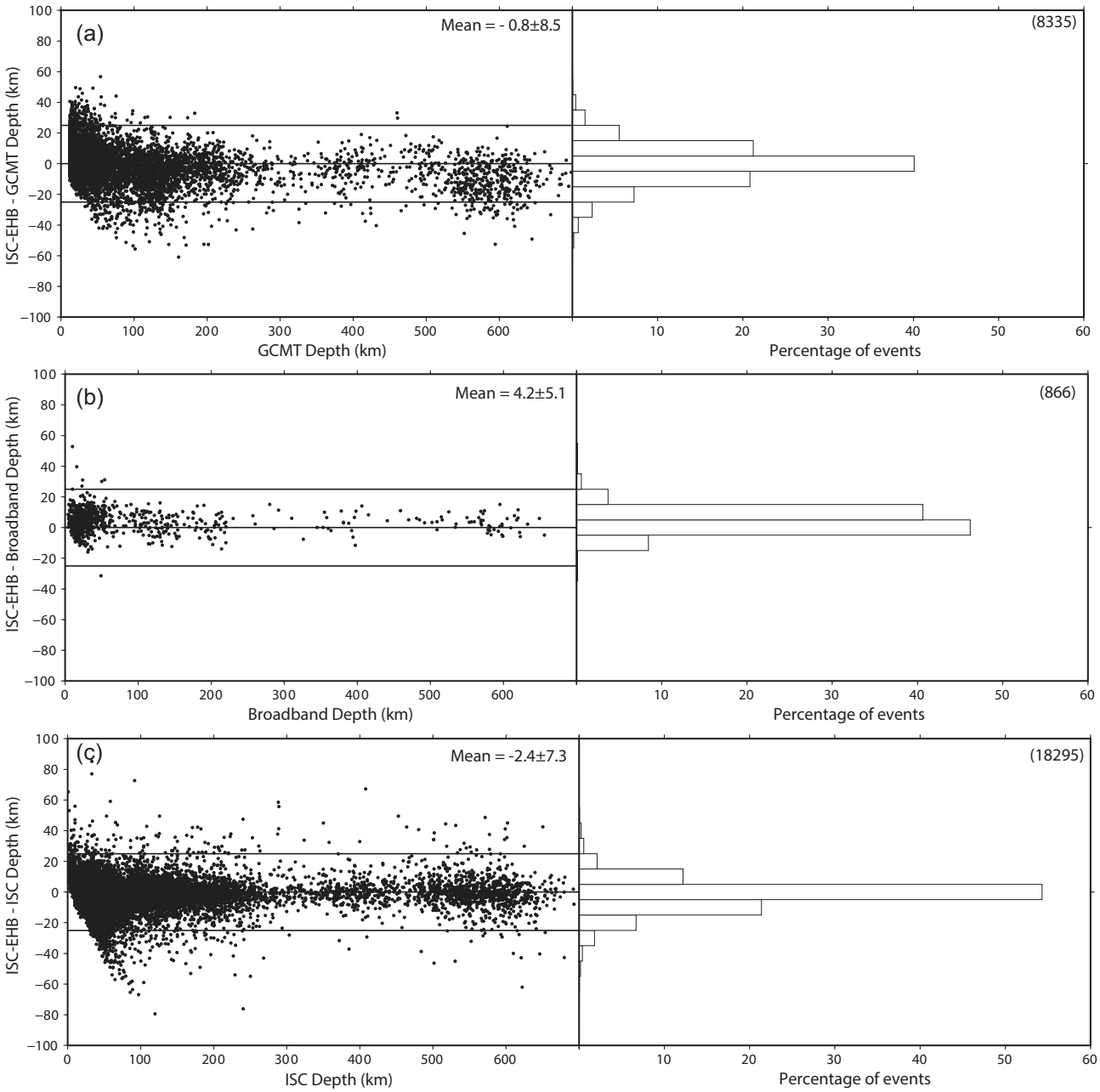

Figure 10. (a) Difference plot to compare ISC-EHB depths with (a) GCMT depths, (b) USGS broad-band depths and (c) ISC depths. It should be noted that only ISC-EHB events in the L1 depth category are used in the comparisons. The black lines in the left-hand plot in (a)–(c) correspond to −25, 0 and 25 km depth differences, and the mean difference is shown in the top right of the plot. The *y*-axis on the right-hand plot in (a)–(c) shows the percentage of events in 10 km bins, where the total number of events in each plot is shown in brackets in the top right.The mean bias for GCMT and broad-band depths is probably due to the different frequencies of depth phase waveforms (long period, broad-band and high-frequency, respectively). The bias for ISC depths is that they are largely overestimated for shallow events.

deviations) for L1 events, based on the comparison to GCMT and broad-band depths.

4.3 Review issues

Manual review of cross-sections can vary in difficulty. For example, some cross-sections such as Hindu Kush are relatively straightforward to assess in cross-section as the subducting slab structure is clearly defined and therefore outliers are easier to identify (Fig. 11b). However, in other regions where the tectonic structure is more complex and there are large numbers of events, such as in Indonesia, it is harder to decide which events may need reviewing and there are too many of them to manually review on an individual basis (Fig.11d).

4.4 Sharper definition of structures

Changes in slab morphology with depth are observed in many subduction zones around the world, and imaging them is important for better understanding subduction zone behaviour. One new aspect

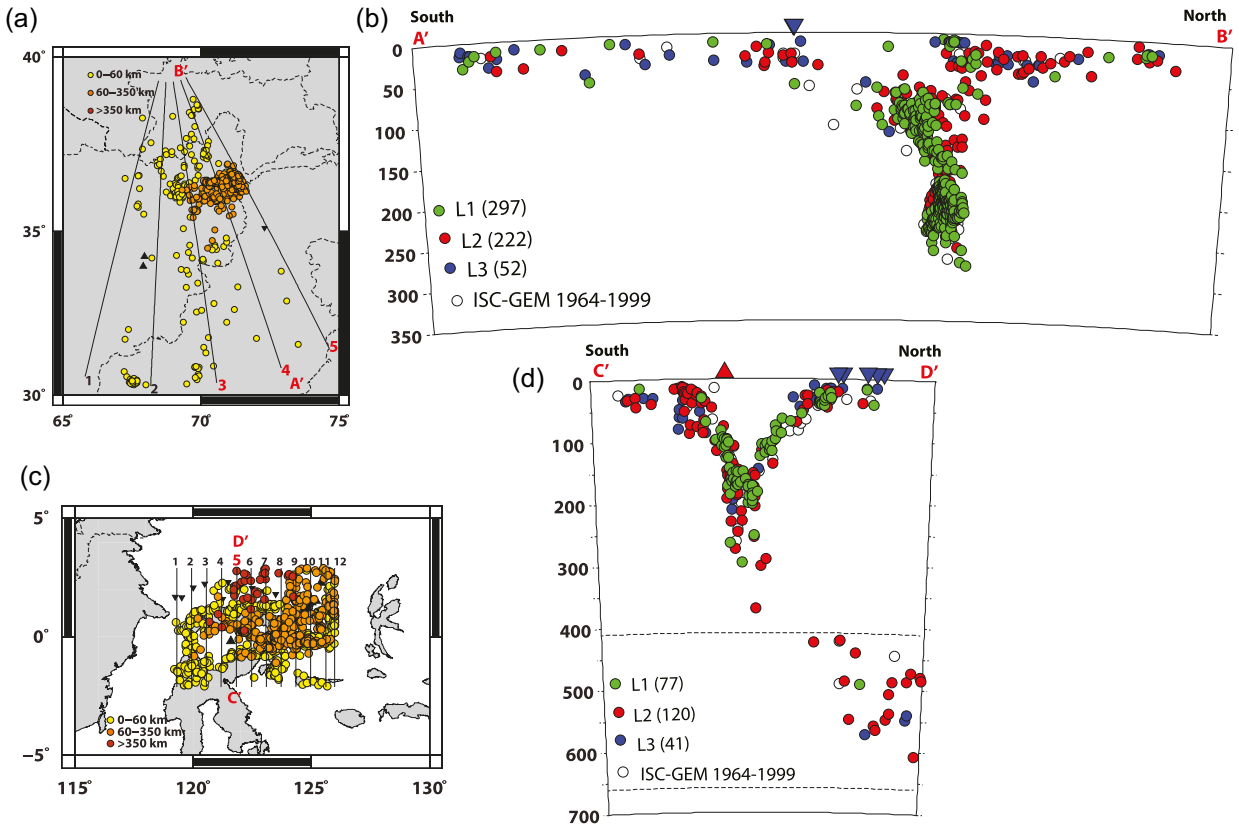

Figure 11. Two example maps and cross-sections to illustrate review issues, most notably the difficulty in identifying outliers. (a) Map of the Hindu Kush region split up into five cross-sections. The trench here is the Himalayan Front where the Indian plate begins subducting beneath the Eurasian plate. (b) Cross-sections 3–5 combined into one cross-section, the extent of which is indicated by A' and B' in (a). (c) Map of Sulawesi region split up into 12 cross-sections. (d) Cross-section 5, which is denoted by C' and D' in (c). Symbols and colours follow same convention as in Fig. 3.

to the ISC-EHB is the release of the cross-sections which we hope will be a useful source of information when investigating regional tectonics. The latest data set shows some clearly defined structures in subduction zones globally, which have been the subject of many previous studies. Between the Vanuatu and Fiji-Tonga subduction zones an active region of deep seismicity (450–650 km) is well-documented, sometimes referred to as the Vityaz earthquakes (Sykes 1966; Giardini 1992; Okal & Kirby 1998). It has been suggested that this seismicity could be due to a mobile stagnant slab (Okal 2001; Wu *et al.* 2017). Looking at the cross-sections for this region (Fig. 12b), there is a clear flat structure at depth which supports the hypothesis of a flat stagnant slab.

Similarly, the structure of the Tonga subduction zone is the focus of much research in part due to its rapid rate of subduction (~200 mm yr^{-1} e.g. Bevis *et al.* 1995). Numerous earthquake hypocentre and regional tomographic studies in this region have reported that the cold slab sinks steeply and at depth there is a remnant slab (e.g. Hanuš & Vaněk 1979; Chen & Brudzinski 2001; Brudzinski & Chen 2003). The ISC-EHB events in cross-sections for this area (Fig. 12d) agree with these observations; a clear consistently steep dip is seen up to 500 km and below this the dip is steeper and a potential slab break off is suggested by the relocated events.

We also observe flat slab subduction in our data set, which is another topic of much research due to the debate surrounding the causes of flat slab subduction. The Peruvian flat slab has been widely studied regarding the change in dip along-strike and down-dip. (e.g. Barazangi & Isacks 1976; Cahill & Isacks 1992; Gutscher *et al.* 2000). Combining cross-sections in Peru in this study, a flat slab is evident with a downturn in depth at the eastern end and the deeper seismicity appears to have different orientation (Fig. 12f).

4.5 Aftershock sequences

One of the most notable earthquakes during the 2000–2013 period was the M_w 9.0 2011 March 11 Tohoku-oki earthquake. Consequently, 2011 has the greatest number of earthquakes in the ISC-EHB, as a large number of aftershocks following this event are included in this data set. A number of these events that are well-constrained in depth are located beneath the thrust zone (Fig. 5b) and clearly highlight the lower plane of the double seismic zone, albeit lower magnitude events, that has been observed beneath northern Honshu (Hasegawa *et al.* 1979; Kawakatsu & Seno 1983).

5 CONCLUSIONS

We have developed, tested and applied a new approach for selecting and processing ISC Bulletin events to produce the ISC-EHB, a robust data set for tomographic and tectonic studies. The resulting

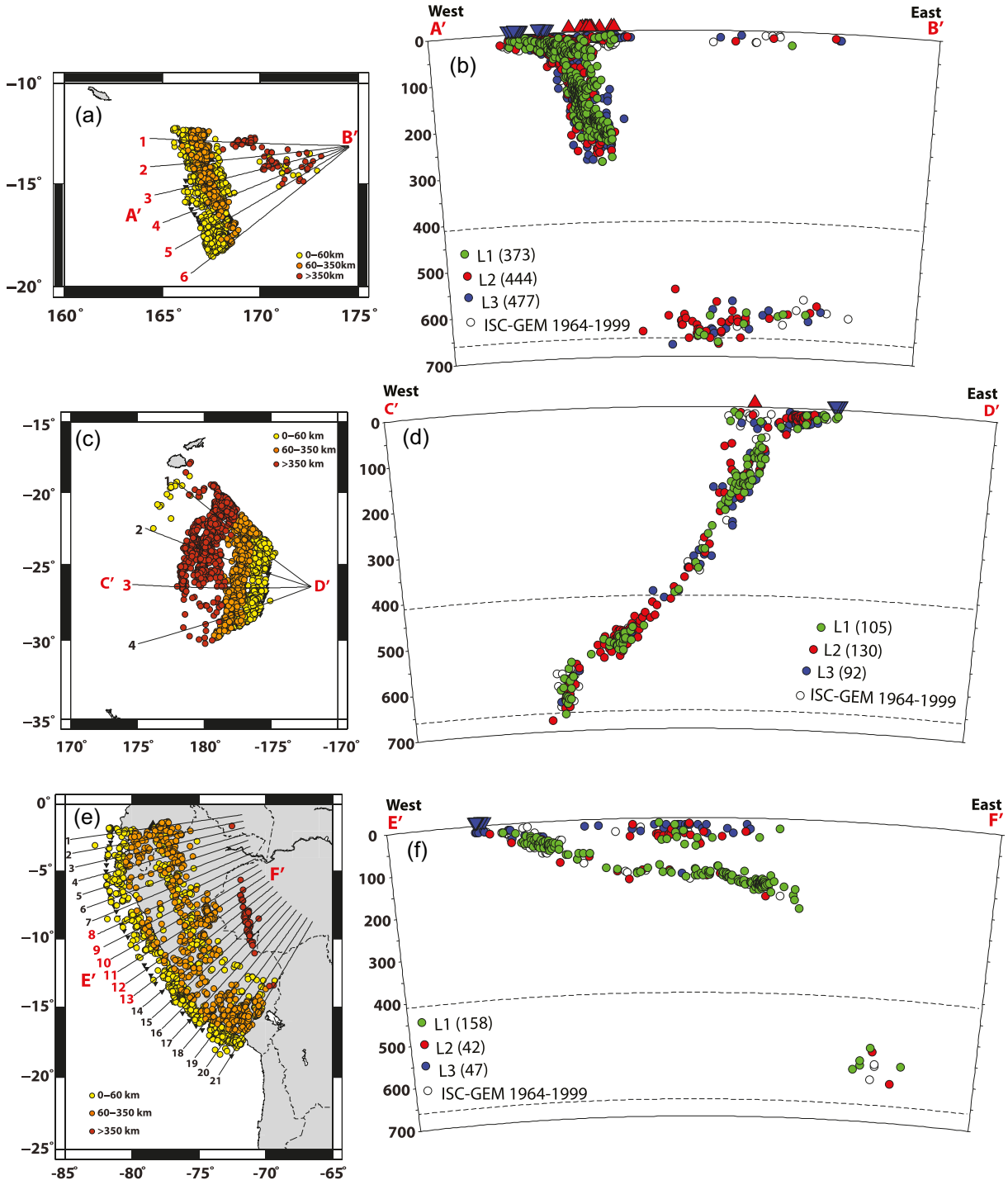

Figure 12. Deep structure of subduction zones. (a) Map of cross-sections for the Vanuatu subduction zone. (b) Combination of all six cross-sections to show a potential foundered slab at depth, the location and extent of the cross is denoted by A' and B' in (b). (c) Map of cross-sections for southern Vanuatu region. (d) Cross-section 3 (C' to D' in (c)) to demonstrate how the structure of the slab changes from 0 to 700 km depth. (e) Map of cross-sections for Peru. (f) Combination of six cross-sections (8–13, denoted by E' to F' in (e)) to show flat slab structure. Symbols and colours follow same convention as in Fig.3.

data set for events between 2000 and 2013 shows improved resolution of clusters of seismicity and sharper definition of subducting slabs, and an improved view of global seismicity relative to other routinely produced catalogues is achieved. These new ISC-EHB procedures will next be applied to events between 1964 and 1999, as well as 2014 and beyond, to produce a consistent data set that will span more than 50 yr.

ACKNOWLEDGEMENTS

We would like to thank the reviewers Guust Nolet and Gavin Hayes for their comments and suggestions, which really helped in improving this manuscript. We acknowledge the financial support from 64 member-institutions of the ISC, as well as dedicated support from NSF (Award 1417970). We thank the research and operation institutions around the world for the regular supply of seismic bulletins to

the ISC. The figures were generated using the Generic Mapping Tool (GMT, Wessel & Smith 1998). Regarding author contributions, JH, ERE and JW selected and processed the data. ERE and JW reviewed the events to produce the ISC-EHB. ERE, JW and DDG analysed results of the ISC-EHB. JW and ERE wrote the manuscript with contributions from JH, DDG and DAS.

REFERENCES

Barazangi, M. & Isacks, B., 1976. Spatial distribution of earthquakes and subduction of the Nazca plate beneath South America, *Geology,* **4**(11), 686–692.

Bevis, M. *et al.*, 1995. Geodetic observations of very rapid convergence and bark-arc extension at the Tonga arc, *Nature,* **374,** 249–251.

Bondar, I., Bergman, E., Engdahl, E., Kohl, B., Kung, Y.-L. & McLaughlin, K., 2008. A hybrid multiple event location technique to obtain ground truth event locations, *Geophys. J. Int.,* **175**(1), 185–201.

Bondar, I., Myers, S., Engdahl, E. & Bergmann, E., 2004. Epicentre accuracy based on seismic network criteria, *Geophys. J. Int.,* **156**(3), 483–496.

Bondar, I. & Storchak, D., 2011. Improved location procedures at the International Seismological Centre, *Geophys. J. Int.,* **186**(3), 1220–1224.

Brudzinski, M. & Chen, W., 2003. A petrologic anomaly accompanying outboard earthquakes beneath Fiji-Tonga: corresponding evidence from broadband *P* and *S* waveforms, *J. geophys. Res.,* **108**(B6), doi:10.1029/2002JB002012.

Cahill, T. & Isacks, B., 1992. Seismicity and shape of the subducted Nazca plate, *J. geophys. Res.,* **97**(B12), 17 503–17 529.

Chen, W. & Brudzinski, M., 2001. Evidence for a large-scale remnant of subducted lithosphere beneath Fiji, *Science,* **295,** 2475–2479.

Choy, G. & Engdahl, E., 1987. Analysis of broadband seismograms from selected IASPEI events, *Phys. Earth planet. Inter.,* **47,** 80–92.

Di Giacomo, D. & Storchak, D., 2016. A scheme to set preferred magnitudes in the ISC bulletin, *J. Seismol.,* **20**(2), 555–567.

Duarte, J. & Schellart, W., 2016. *Plate Boundaries and Natural Hazards,* John Wiley & Sons.

Ekström, G., 2006. Global detection and location of seismic sources by using surface waves, *Bull. seism. Soc. Am.,* **96**(4A), 1201–1212.

Engdahl, E., Taggart, J., Lobdell, J., Arnold, E. & Clawson, G., 1968. Computational methods, *Bull. seism. Soc. Am.,* **58**(4), 1339–1344.

Engdahl, E., van der Hilst, R. & Buland, R., 1998. Global teleseismic earthquake relocation with improved travel times and procedures for depth determination, *Bull. seism. Soc. Am.,* **88**(3), 722–743.

Engdahl, E., Villasenor, A., DeShon, H. & CH., T., 2006. Teleseismic relocation and assessment of seismicity (1918–2005) in the region of the 2004 M_w 9.0 Sumatra–Anadaman and 2005 M_w 8.6 Nias Island Great earthquakes, *Bull. seism. Soc. Am.,* **97,** S43–S61.

Giardini, D., 1992. Space–time distribution of deep seismic deformation in Tonga, *Phys. Earth planet. Inter.,* **74,** 75–88.

Gutscher, M.-A., Spakman, W., Bijwaard, H. & Engdahl, E., 2000. Geodynamics of flat subduction: seismicity and tomographic constraints from the Andean margin, *Tectonics,* **19,** 814–833.

Hanuš, V. & Vaněk, J., 1979. Morphology and volcanism of the Wadati–Benioff zone in the Tonga-Kermadec system of recent subduction, *N.Z. J. Geol. Geophys.,* **22,** 659–671.

Hasegawa, A., Umino, N., Takagi, A. & Suzuki, Z., 1979. Double-planed deep seismic zone and anomalous structure in the upper mantle beneath northeastern Honshu, *Tectonophysics,* **57,** 1–6.

Hayes, G., Wald, D. & Johnson, R., 2012. Slab1.0: A three-dimensional model of global subduction zone geometries, *J. geophys. Res.,* **117**(B1), doi:10.1029/2011JB008524.

Herrin, E. & Taggart, J., 1968. Source bias in epicenter determinations, *Bull. seism. Soc. Am.,* **58,** 1791–1796.

Huang, J. & Zhao, D., 2006. High-resolution mantle tomography of China and surrounding regions, *J. geophys. Res.,* **111**(B9), doi:10.1029/2005JB004066.

ISC, 2018. International Seismological Centre: On-line Bulletin. *International Seismological Centre,* UK, http://www.isc.ac.uk.

Kawakatsu, H. & Seno, T., 1983. Triple seismic zone and the regional variation of seismicity along the Northern Honshu Arc, *J. geophys. Res.,* **88**(B5), 4215–4230.

Kennett, B., Engdahl, E. & Buland, R., 1995. Constraints on seismic velocities in the Earth from traveltimes, *Geophys. J. Int.,* **108,** 108–124.

Li, C., van der Hilst, E., Engdahl, E. & Burdick, S., 2008. A new global model for *P*-wave speed variations in Earth's mantle, *Geochem. Geophys. Geosyst.,* **9**(5), doi:10.1029/2007GC001806.

Montelli, R., Nolet, G., Dahlen, F., Masters, G., Engdahl, E. & Sung, S., 2004. Finite-frequency tomography reveals a variety of plumes in the mantle, *Science,* **303,** 338–343.

Myers, S. & Schultz, C., 2000. Calibration of seismic travel time using events with seismically determined locations and origin times, *EOS, Trans. Am. geophys. Un.,* **81,** F845.

Okal, E., 2001. "Detached" deep earthquakes: are they really? *Phys. Earth planet. Inter.,* **127,** 109–143.

Okal, E. & Kirby, S., 1998. Deep earthquakes beneath the Fiji Basin, SW Pacific: Earth's most intense deep seismicity in stagnant slabs, *Phys. Earth planet. Inter.,* **109**(1–2), 25–63.

Pesicek, J., Engdahl, E., Thurber, C.H., DeShon, H. & Lange, D., 2012. Mantle subducting slab structure in the region of the 2010 M 8.8 Maule earthquake (30-40s), chile, *Geophys. J. Int.,* **191**(1), 317–324.

Schmid, C., van der Lee, S., VanDecar, J., Engdahl, E.R. & Giardini, D., 2008. Three-dimensional S velocity of the mantle in the Africa-Eurasia plate boundary region from phase arrival times and regional waveforms, *J. geophys. Res.,* **113,** B03306, doi:10.1029/2005JB004193.

Siebert, L. & Simkin, T., 2002. *Volcanoes of the World: an Illustrated Catalog of Holocene Volcanoes and Their Eruptions,* Global Volcanism Program Digital Information Series.

Storchak, D., Di Giacomo, D., Engdahl, E., Harris, J., Bondar, I., Lee, W., Bormann, P. & Villasenor, A., 2015. The ISC-GEM Global Instrumental Earthquake Catalogue (1900–2009): introduction, *Phys. Earth planet. Inter.,* **239,** 14–24.

Storchak, D., Harris, J., Brown, L., Lieser, K., Shumba, B., Verney, R., Di Giacomo, D. & Korger, E., 2017. Rebuild of the bulletin of the International Seismological Centre (ISC) part 1: 1964–1979, *Geosci. Lett.,* **4**(1), 32, doi:10.1186/s40562-017-0098-z.

Sykes, L., 1966. The seismicity and deep structure of Island arcs, *J. geophys. Res.,* **71**(12), 2981–3006.

Waldhauser, F., Schaff, D.P., Diehl, T. & Engdahl, E., 2012. Splay faults imaged by fluid driven aftershocks of the 2004 M_w 9.2 Sumatra–Andaman earthquake, *Geology,* **40**(3), 243–246.

Wessel, P. & Smith, W., 1998. New, improved version of the generic mapping tools released, *EOS, Trans. Am. geophys. Un.,* **79,** 579.

Wu, J., Suppe, J., Lu, R. & Kanda, R., 2017. Stagnant slab tectonics of the Japan and northern Tonga slabs, in *JpGU-AGU Joint Meeting,* Kobe, August 2017.